Available online at www.sciencedirect.com
ScienceDirect
Ceramics International 35 (2009) 2837–2844
CERAMICS INTERNATIONAL
www.elsevier.com/locate/ceramint

Effect of polyvinylpyrrolidone on morphology and structure of In_2O_3 nanorods by hydrothermal synthesis

Tzu-Tsung Tseng, Wenjea J. Tseng *

Department of Materials Science and Engineering, National Chung Hsing University, 250 Kuo Kuang Road, Taichung 402, Taiwan

Received 19 December 2008; received in revised form 2 March 2009; accepted 18 March 2009
Available online 15 April 2009

Abstract

Indium oxide (In_2O_3) nanorods were hydrothermally synthesized from aqueous $InCl_3$ solution in urea with addition of polyvinylpyrrolidone (PVP) as a steric stabilizer. Indium hydroxide, $In(OH)_3$, was precipitated at 60 °C and was changed into a transient InOOH phase upon calcination at ~250 °C in air. X-ray diffractometry revealed that the existence of PVP delays the phase transformation of InOOH. Cubic-structured In_2O_3 phase was then formed when temperature was raised to 350 °C, regardless of the PVP concentration. The $In(OH)_3$ phase without the PVP showed a rod-based, flower-like morphology of polycrystalline character. Minor addition of the PVP, i.e., 0.1–2 wt.%, resulted in a pronounced evolution in morphology from the three-dimensional, flower-like form to discrete, one-dimensional nanorods aligned in planar form. Both the flower-like and discrete nanorod morphologies were preserved after heat treatments at 250 and 350 °C. This reveals that the morphological change is attributable to preferential adsorption of the PVP molecules on the $In(OH)_3$ crystallite surface, so that the aggregate attachment responsible for the multipod growth is inhibited.

Keywords: Indium oxide (In_2O_3); Nanorod; Structure

1. Introduction

Semiconductive indium oxide (In_2O_3) with a wide bandgap (direct bandgap around 3.6 eV at room temperature) has attracted much attention in recent years, owing mainly to its application in solar cell [1], field-emission display [2], lithium-ion battery [3], nanoscale biosensor [4], gas sensor [5], optoelectronics [6], and photocatalysis [7]. In_2O_3 nanorods and nanowires with tailored morphology, architecture and surface functionality, in particular, present unique anisotropic properties that respond readily to minute changes in specific external stimuli, giving rise to a selective recognition capability and an improved device stability [4,8–10]. In view of the literature, In_2O_3 crystals of various morphologies have been prepared by different physical and chemical routes. For example, Pan et al. first synthesized one-dimensional In_2O_3 nanobelts through thermal evaporation [11]. Highly oriented In_2O_3 nanowires and branched nanostructures were grown by vapor–liquid–solid (VLS) mechanism [12] and by chemical vapor deposition (CVD) [13,14]. The CVD-grown In_2O_3 nanostructures with morphologies such as octahedral nanoparticle, nanochain, nanobelt, nanosheet, and nanowire were obtained by properly tuning the synthesis variables [13]. In addition, arrays of vertically aligned In_2O_3 nanorods and nanowires have been fabricated by physical means via template-assisted growth, within which the growth direction of In_2O_3 crystals is virtually confined to pre-defined pore channels with specific orientations [6,15,16].

Apart from the physical methods, In_2O_3 nanorods have been prepared via chemical means, such as sol–gel [17], chemical precipitation [18,19], forced hydrolysis [20], solvothermal synthesis [21,22], sonohydrolysis [23], and hydrothermal synthesis [24–26]. Preparation of one-dimensional In_2O_3 crystals with desired nanostructure and morphology is advantageous from both time- and cost-perspectives when chemical routes are employed. Use of sacrificial templates and organic surfactants to facilitate the anisotropic growth of In_2O_3 nanorods in solutions, in particular, has received much attention recently [10,17,22,25,27–29]. For example, Cheng et al. [17] used polyethylene octylphenylether as a directing surfactant for

* Corresponding author. Fax: +886 4 2285 7017.
E-mail address: wenjea@dragon.nchu.edu.tw (W.J. Tseng).

0272-8842/$36.00
doi:10.1016/j.ceramint.2009.03.028

synthesizing In_2O_3 nanorods via a sol–gel route. The presence of polymeric surfactant changed the shape of In_2O_3 nanocrystals from sphere to rod, ascribing presumably to the micelle conformation of the surfactant molecules. Du et al. [22] examined morphological change of $In(OH)_3$ when surfactants of ethylenediamine, acetic acid, and oleic acid were used in their solvothermal synthesis, respectively. Well-crystalline $In(OH)_3$ nanospheres, nanoflowers, microcubes, and nanorods were produced when different surfactants and surfactant concentrations were used. Their findings revealed that the nucleation and growth of $In(OH)_3$ crystallites were predominately influenced by the adsorption of surfactant molecules over preferential binding sites on the crystallite surface so that the oriented aggregate attachment at the active corners of the primary crystallites is operative to facilitate the formation of $In(OH)_3$ crystals to various morphologies. In_2O_3 crystals of similar geometry were retained after calcination of the $In(OH)_3$ products at elevated temperatures. In addition, $In(OH)_3$ and In_2O_3 nanocrystals with morphologies of nanorod bundles and spherical agglomerates were also formed when cetyltrimethylammonium bromide (CTAB) was used as a surfactant in microemulsion-mediated hydrothermal synthesis [25]. The presence of CTAB gave rise to formation of In_2O_3 single crystals with a well-defined cubic morphology [10]; to which, a typical Ostwald ripening was suspected responsible for the growth of In_2O_3 nanocubes.

Huang and Gao [28] recently synthesized $In(OH)_3$ precipitates with a range of shapes in ethanol/water solvents, and found that the anisotropic growth of $In(OH)_3$ precipitates was facilitated by polyvinylpyrrolidone (PVP) molecules which preferentially adsorbed on the $In(OH)_3$ crystallites. Zhang et al. [29] then prepared In_2O_3 nanofibers by electrospinning indium precursors consisting of PVP as a structure-directing agent in water/ethanol solvents. Even though PVP has been widely used as a capping agent and a surfactant as well in controlling the growth and structure of various one-dimensional ceramics and metals via the solution-based synthesis routes [28–37], relevant reports are yet rare for the formation of In_2O_3 nanorods specifically. In this paper, In_2O_3 nanorods were synthesized from $In(OH)_3$ prepared hydrothermally in the presence of PVP polymers with concentrations up to 2 wt.%. The formation, morphology, and structure of the In_2O_3 nanorods were examined by thermogravimetric and differential thermal analyses (TG/DTA), Fourier transform infrared spectrometry (FTIR), X-ray diffractometry (XRD), and electron microscopy, with an aim that the influence of PVP polymers on the hydrothermally prepared In_2O_3 nanorods is elucidated.

2. Experimental procedure

2.1. Synthesis

Anhydrous indium chloride ($InCl_3$, 99.99%, Alfa, USA) and analytical-grade urea (BP, Riedel-de Haen, Germany) were used as-received without further purification, and were dissolved in pure water (18.3 MΩ). The indium and urea

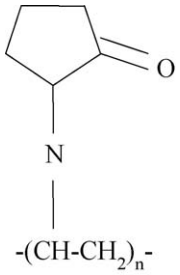

Fig. 1. The molecular structure of PVP polymer.

concentrations were kept at 5×10^{-5} and 0.1 M, respectively. Reagent-grade PVP (molecular weight 360,000, Sigma, USA) with a molecular structure shown in Fig. 1 was then added to the solutions. The PVP concentration ranged from 0 to 2 wt.%. The solutions were kept at 60 °C for 8 h with a continuous agitation before being subjected to ice water to terminate the reaction. Whitish precipitates were collected from the solutions by centrifugation at 10,000 rpm and the settled particles were rinsed and washed in pure water ultrasonically for three times. The precipitates were then oven-dried at 50 °C before being calcined to 250–350 °C in a tube furnace (Thermolyne, Barnstead International, USA) at a heating rate of 10 °C min^{-1} 1 in flowing air atmosphere.

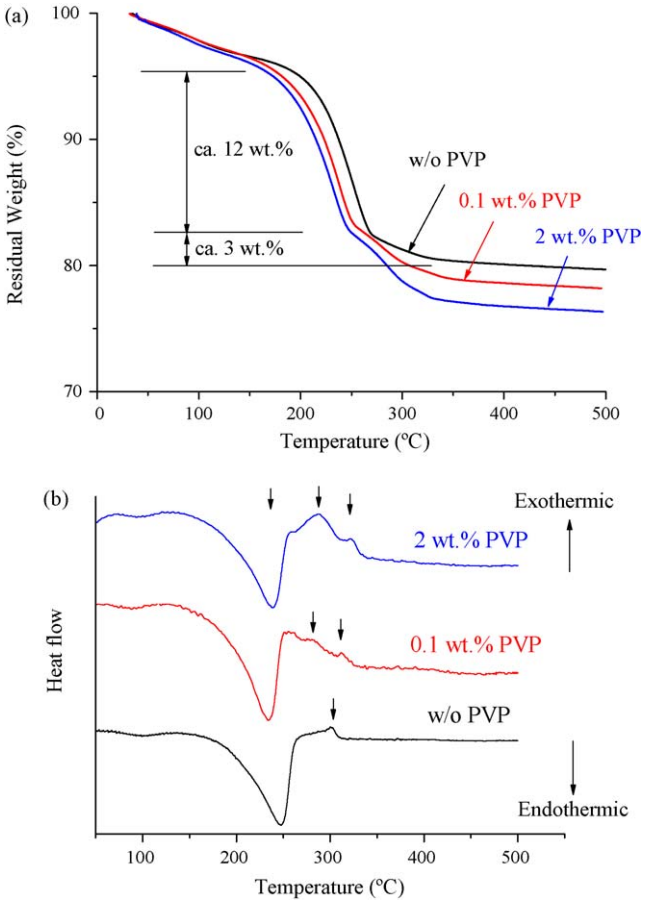

Fig. 2. TGA (a) and DTA (b) curves of the precipitated particles synthesized at different PVP concentrations.

2.2. Characterization

Thermogravimetric and differential thermal analyses (TG/DTA, Diamond 6300, Perkin Elmer, USA) were used to examine the precipitated indium-hydroxide particles at elevated temperatures. The powdered samples were placed in alumina crucibles, and heated to 400 °C in flowing air atmosphere at a heating rate of 10 °C min^{-1}. Structure of the precipitates was characterized by X-ray diffractometry (XRD, MAC MXP III, Japan) using Cu Kα radiation with a wavelength of 1.5406 Å. Some of the precipitated powders were mixed with KBr powders in a constant weight ratio of 1:10, and their characteristic absorptions were determined by FTIR in transmittance mode (Spectrum RX-I, Perkin Elmer, USA) over a wavenumber range of 400–4000 cm^{-1}. Morphology and microstructure of the calcined particles were examined by both field-emission scanning electron microscopy (FESEM, JSM-6700F, JEOL, Japan) and transmission electron microscopy (TEM, JEM-2010, JEOL, Japan).

3. Results and discussion

Fig. 2 shows thermal degradation of the hydrothermally prepared indium-hydroxide precipitates with various PVP concentrations. Weight loss occurs gradually at temperature above room temperature and reaches ∼5% around 200 °C in Fig. 2(a). This weight reduction is due to the loss of absorbed water (mainly from hydration of the indium chloride used as the starting material) [17] and thermal decomposition of the surfactant polymer. A significant weight loss (∼12%) follows at ∼200–250 °C with an apparent endothermic peak (Fig. 2(b)). This is attributable to the phase transformation from $In(OH)_3$ to InOOH; to which, a comparable weight loss of 10.9% is calculated from the following reaction:

$$In(OH)_3 \rightarrow InOOH + H_2O \quad (1)$$

A weak exothermic peak is found at ∼300 °C for the indium-hydroxide synthesized without PVP (Fig. 2(b)). This is presumably ascribed to the formation of In_2O_3 from InOOH [37], i.e.,

$$2InOOH \rightarrow In_2O_3 + H_2O \quad (2)$$

A theoretical estimate of 6.1% weight loss would accompany this reaction, which is slightly larger than our experimental finding (∼3%) in Fig. 2(a). Cheng et al. [17] have reported that formation of In_2O_3 nanorods directly from $In_2O(OH)_4$ gelatin via a sol–gel route would occur at 263 °C when $InCl_3$ was used as a precursor. One might hence suspect that some $In(OH)_3$

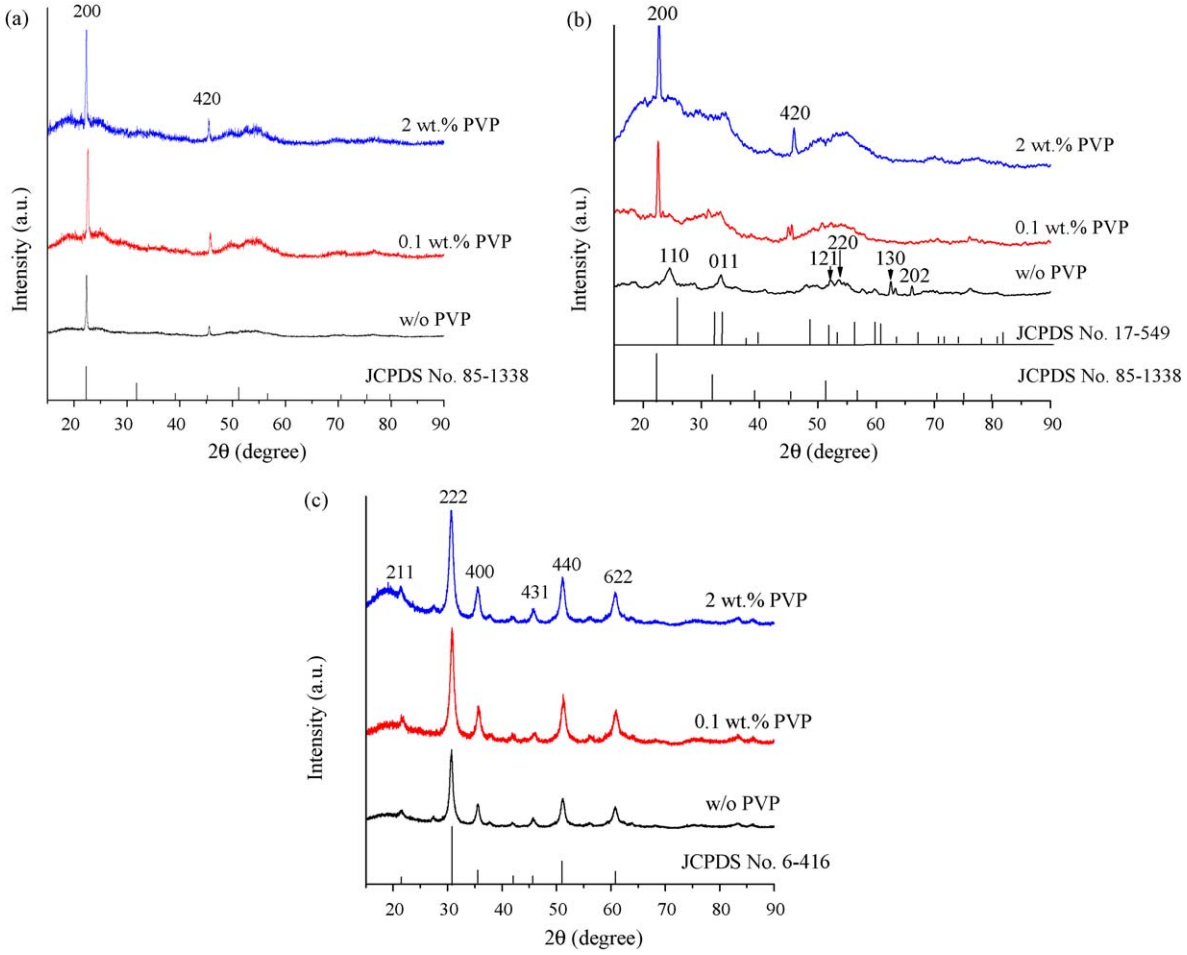

Fig. 3. XRD patterns of hydrothermally synthesized indium-hydroxide precipitates with various PVP concentrations (a) prior the calcinations process, and pyrolyzed at (b) 250 °C, and (c) 350 °C.

might have formed In_2O_3 phase at the lower temperature region (~200–250 °C) since

$$2In(OH)_3 \rightarrow In_2O_3 + H_2O \quad (3)$$

This reaction involves a theoretical weight loss of 16.3%. Therefore, a more pronounced weight loss at the temperature range ~200–250 °C would result, whilst a reduced weight reduction follows upon further increase of temperature above ~300 °C. In addition, a more pronounced weight loss (about 4–6%) is found for the indium hydroxides with PVP in Fig. 2(a). The additional weight reductions are due to the degradation of PVP polymers at temperature near 300 °C [29]; along which, an apparent exothermic peak also results (Fig. 2(b)).

Fig. 3 shows XRD patterns of the hydrothermally prepared indium-hydroxide precipitates calcined at various temperatures. The precipitates all show a cubic $In(OH)_3$ phase (JCPDS No. 85-1338) after hydrothermal reaction at 60 °C in Fig. 3(a), regardless of the PVP concentration. The poor crystallinity of the $In(OH)_3$ phase is indicative of partial formation of crystalline $In(OH)_3$ phase at the relatively low reaction temperature employed. In addition, the disappearance of (2 2 0), (2 2 2), and (4 0 0) reveals the preferential growth of $In(OH)_3$ crystallites along predominately ⟨1 0 0⟩ crystallographic directions [26,28]. In Fig. 3(b), the presence of PVP molecules appears to delay the formation of InOOH phase (JCPDS No. 17-549) when the $In(OH)_3$ precipitates were heated to 250 °C. The exact mechanism is not clear at present, but we suspect that the preferentially adsorbed PVP molecules on specific planes of the $In(OH)_3$ crystallites might have contributed to the phase transformation from $In(OH)_3$-to-InOOH to an undetermined extent. When temperature is further raised to 350 °C, at which all the PVP was totally removed thermally, all the indium hydroxides become cubic-structured In_2O_3 phase (JCPDS No. 6-414) in Fig. 3(c), regardless of the PVP concentrations.

In Fig. 4(a), absorption peaks ascribing to In-OH bonds of the $In(OH)_3$ phase appear at wavenumbers of 531, 645, and 1195 cm^{-1} [35], while N–H and $–CH_2$ bonds of the PVP polymers are at 3380 and 2938 cm^{-1}. These reveal that the PVP molecules adsorbed preferentially on the surface of $In(OH)_3$ crystallites. In Fig. 4(b), the $–CH_2$ bond of PVP decomposes while the N–H bond remains when temperature was raised to 250 °C. The In–O bond emerges at wavenumber of 1638.7 cm^{-1}, suggesting that the phase transformation of $In(OH)_3$-to-InOOH occurs. Disappearance of N–H bond of the PVP polymer at 350 °C in Fig. 4(c) yet indicates a complete removal of the polymer.

The $In(OH)_3$ crystals synthesized at 60 °C show flower-like or planar rod forms, depending on the PVP concentrations. As shown in Fig. 5(a), $In(OH)_3$ nanorods form flower-like, multipod morphology with a size ranging from 600 to 1000 nm without the PVP polymer. The $In(OH)_3$ nanorods appear to detach one another so that the $In(OH)_3$ multipods disappear when PVP concentration was increased to 0.1 wt.% (Fig. 5(b)). The radial dimension and the axial length of the nanorods are about 30 and 200 nm, respectively; to which, both of them are pronouncedly smaller than that of Fig. 5(a) without the PVP addition. As the PVP concentration is further increased

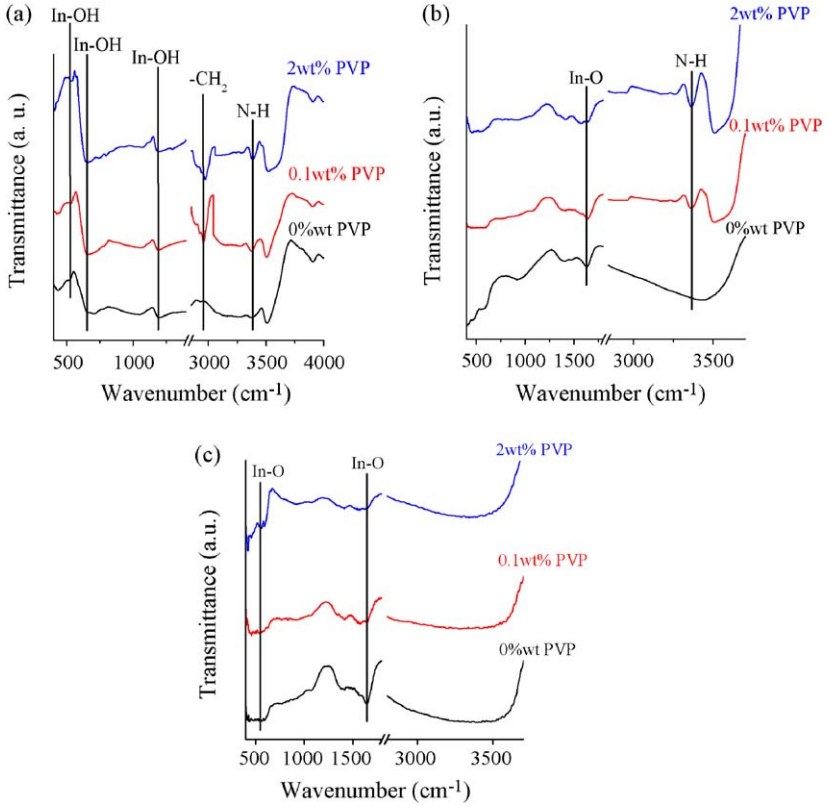

Fig. 4. FTIR spectra of $In(OH)_3$ prepared (a) prior calcination, and calcined at (b) 250 °C, and (c) 350 °C with different PVP concentrations.

to 2 wt.%, the physical dimension of $In(OH)_3$ nanorods does not change much; nonetheless, the morphological configuration of the nanorods becomes planar apparently. Fig. 6 shows In_2O_3 nanorods after heat treatment at 350 °C. Morphologies of the In_2O_3 nanorods are preserved without appreciable change when calcinations temperature was increased above the reaction temperature (60 °C). This indicates that the morphological change is mainly due to the adsorption of PVP molecules on the nucleation and growth of $In(OH)_3$ crystallites in the liquid solvent. Fig. 7 shows TEM structure of the In_2O_3 nanorods.

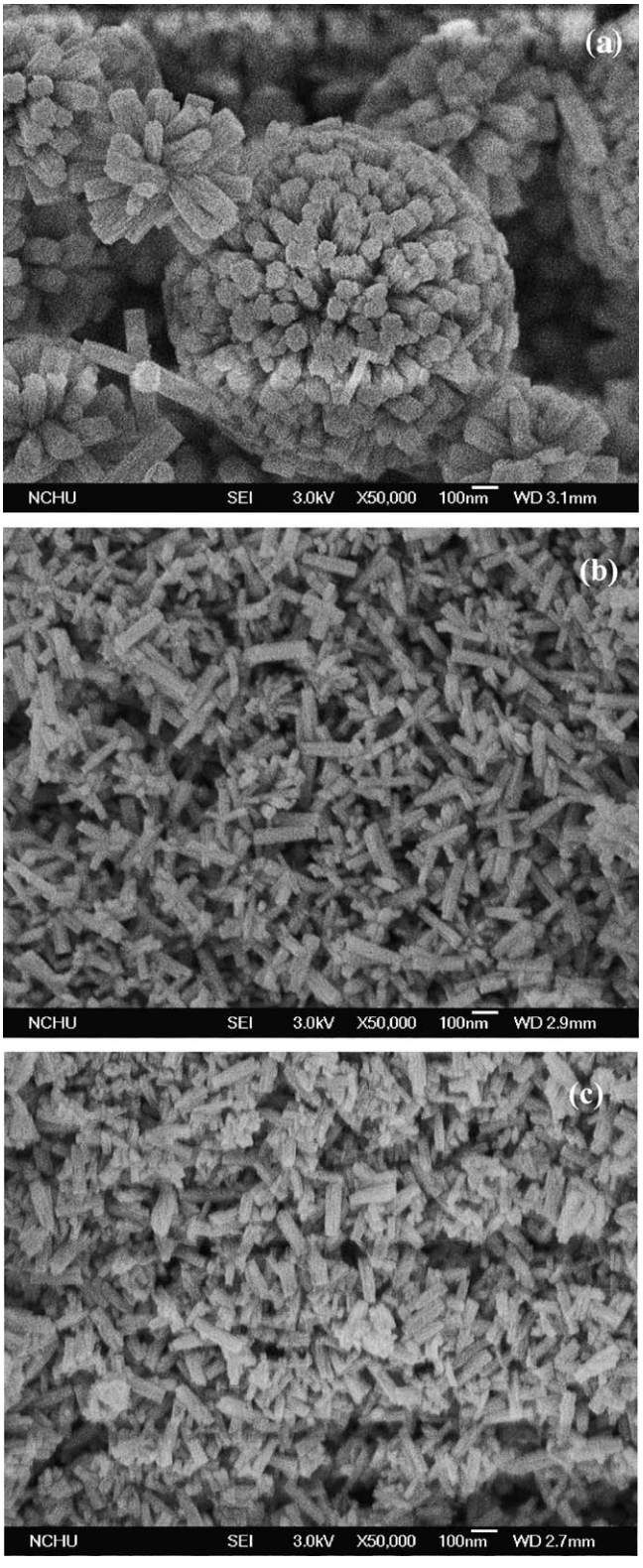

Fig. 5. Morphology of $In(OH)_3$ nanorods with (a) 0 wt.%, (b) 0.1 wt.%, and (c) 2 wt.% PVP prior calcination. Reaction temperature was held at 60 °C.

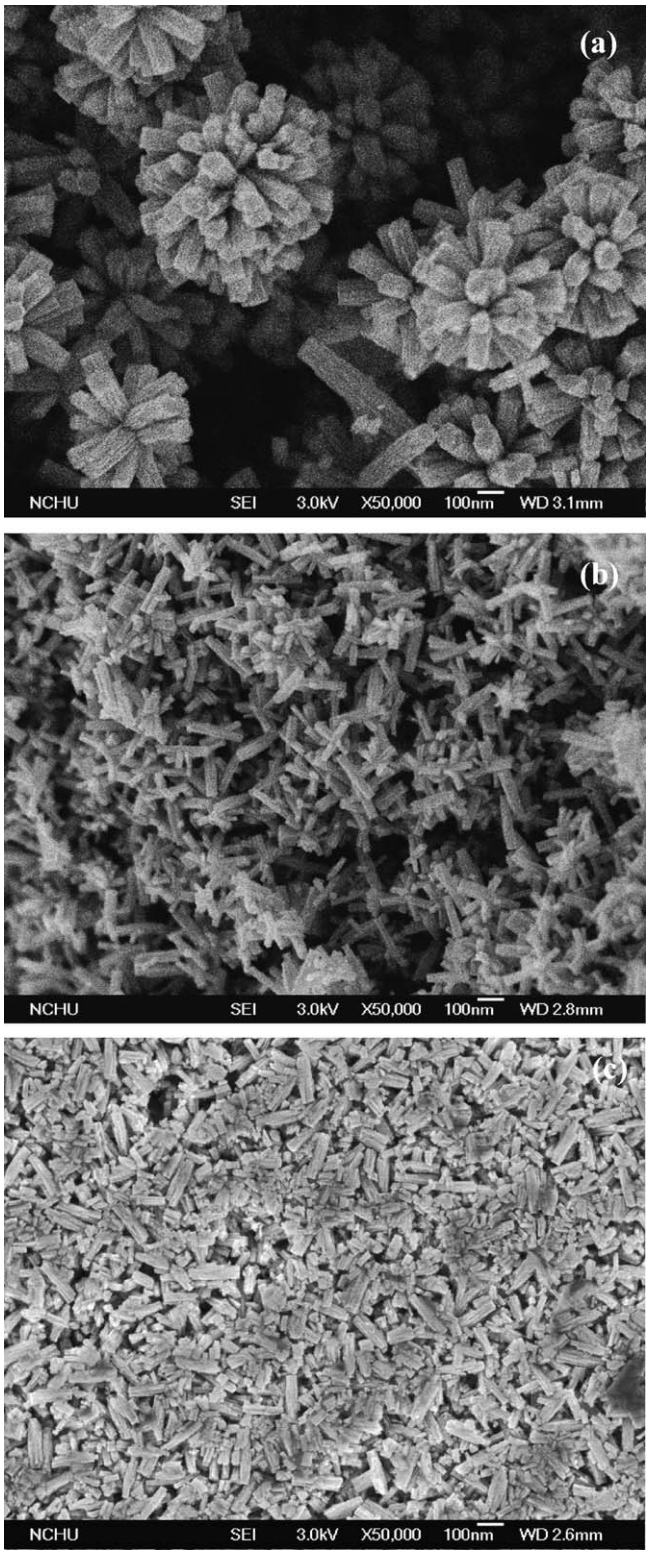

Fig. 6. Morphology of In_2O_3 nanorods with (a) 0 wt.%, (b) 0.1 wt.%, and (c) 2 wt.% PVP after 350 °C calcination in air atmosphere.

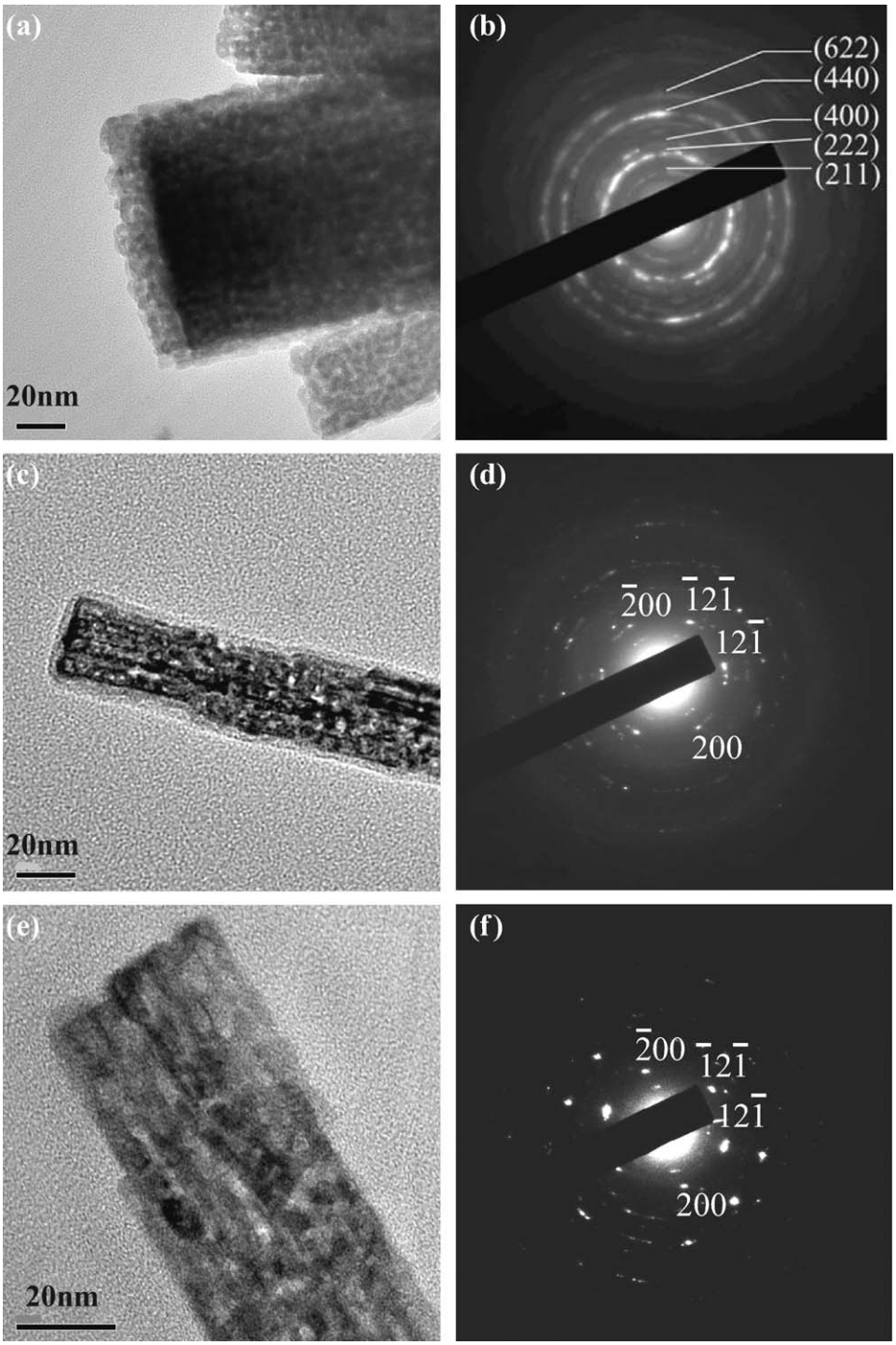

Fig. 7. TEM images of (a) In_2O_3 nanorods without PVP addition, and (b) bcc-structured polycrystalline SAED pattern of (a). (c) TEM images of In_2O_3 nanorods with 0.1 wt.% PVP, and (d) a typical SAED pattern of (c). (e) TEM images of In_2O_3 nanorods with 2 wt.% PVP, and (f) a typical SAED pattern of (e).

Without PVP, the flower-like In_2O_3 nanorods appear to be composed of clustered assemblies of aggregated crystallites (Fig. 7(a)). The concentric Debye rings (Fig. 7(b)) reveal a polycrystalline bcc structure. Yet, the rings are not of uniform intensity around their circumferences, indicative of a high degree of preferred orientations. With PVP additions, the continuous Debye rings become less apparent (Fig. 7(d) and (f)), mainly because of fewer number of crystallite aggregates under electron-beam radiations of identical size.

The growth mechanism for the $In(OH)_3$ nanorods is delineated in Fig. 8. Without PVP, the $In(OH)_3$ nuclei formed in aqueous solution tend to aggregate themselves so that the aggregated attachment is responsible for the multipod growth as temperature is increased. The growth of each nanorod nuclei

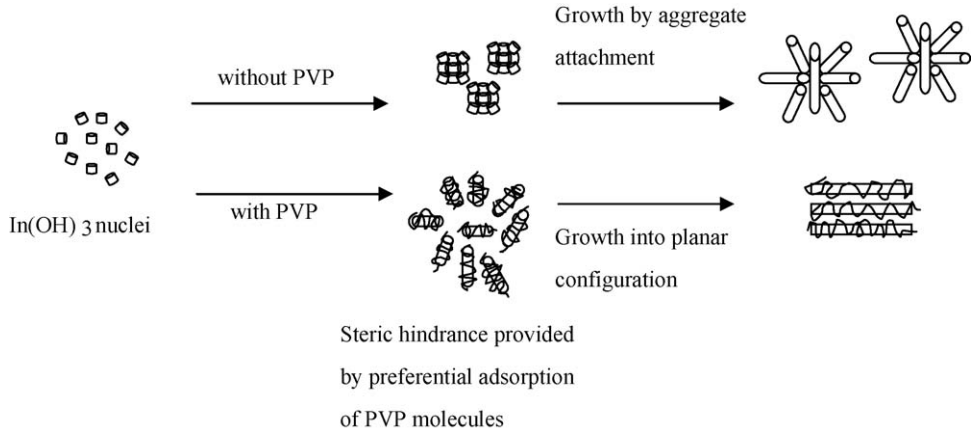

Fig. 8. Schematic of growth mechanism of $In(OH)_3$ nanorods.

is highly anisotropic (predominately along ⟨1 0 0⟩ directions with a minor along ⟨2 1 0⟩ directions); nonetheless, the growth direction of the aggregated cluster as a whole is completely random, leading to the formation of flower-like multipod morphology of polycrystalline character. With PVP, the polymeric molecules would adsorb preferentially on the nuclei surface to inhibit aggregation by steric hindrance mechanism. When the PVP concentration is increased from 0.1 to 2 wt.%, a more complete coverage of the PVP molecules are available to "protect" the neighboring indium hydroxides crystallites from aggregation in liquid, hence leading to a morphology with the co-planar configuration. The growth of $In(OH)_3$ crystallites in the supersaturated liquid medium is believed to have undergone a typical Ostwald ripening process [10,28]; to which, the larger particles grow at the expense of the smaller ones because of the difference in solubility. In addition, it may be interesting to note that the preferential growth directions of the $In(OH)_3$ crystallites are all identical for samples with and without PVP (Fig. 3(a)); therefore, the adsorption of PVP molecules on $In(OH)_3$ crystallites appears unlikely to provide a significant capping effect that would inhibit nucleation and grain growth of the nanorods along specific crystallographic planes while facilitate accelerated growth along other orientations. A recent discovery by Yan et al. [10] found that well-defined $In(OH)_3$ nanocubes were resulted in a urea-based hydrothermal process with addition of CTAB polymers as a capping agent. When PVP was used instead of CTAB, the cubic shape disappeared. This is in good agreement with our experimental findings.

4. Conclusion

PVP molecules adsorb preferentially on $In(OH)_3$ crystallites so that the neighboring crystallites are protected from aggregation by predominately steric hindrance mechanism. This steric effect is suspected the main reason for the eventual formation of In_2O_3 nanorods of different morphologies in the present study. Without the PVP polymer, aggregation of the $In(OH)_3$ crystallites form flower-like clusters in solvent liquids, leading to flower-like multipods at elevated temperatures. With the PVP polymer, the aggregation of $In(OH)_3$ crystallites is prohibited so that the growth of discrete $In(OH)_3$ rods is facilitated. As the PVP concentration increases from 0.1 to 2 wt.%, the surfactant coverage on the $In(OH)_3$ crystallites is believed to be more complete, leading to an eventual formation of planar configuration of In_2O_3 nanorods with a uniform rod diameter and axial length.

Acknowledgment

Financial support from the National Science Council (Taiwan, ROC) under contract number NSC 95-2221-E-005-036-MY3 is gratefully acknowledged.

References

[1] Z.B. Zhou, R.Q. Cui, Q.J. Pang, Y.D. Wang, F.Y. Meng, T.T. Sun, Z.M. Ding, X.B. Yu, Preparation of indium tin oxide films and doped tin oxide films by an ultrasonic spray CVD process, Appl. Surf. Sci. 172 (2001) 245–252.
[2] Y.X. Liang, S.Q. Li, L. Nie, Y.G. Wang, T.H. Wang, In situ synthesis of In_2O_3 nanowires with different diameters from indium film, Appl. Phys. Lett. 88 (2006) 193119.
[3] D.W. Kim, I.S. Hwang, S.J. Kwon, H.Y. Kang, K.S. Park, Y.J. Choi, K. Choi, J.G. Park, Highly conductive coaxial SnO_2–In_2O_3 heterostructured nanowires for Li ion battery electrodes, Nano Lett. 7 (2007) 3041–3045.
[4] M. Curreli, C. Li, Y. Sun, B. Lei, M.A. Gundersen, M.E. Thompson, C. Zhou, Selective functionalization of In_2O_3 nanowire mat devices for biosensing applications, J. Am. Chem. Soc. 127 (2005) 6922–6923.
[5] S. Bianchi, E. Comini, M. Ferroni, G. Faglia, A. Vomiero, G. Sberveglieri, Indium oxide quasi-monodimensional low temperature gas sensor, Sens. Actuators B: Chem. 118 (2006) 204–207.
[6] C.Y. Kuo, S.Y. Lu, T.Y. Wei, In_2O_3 nanorod formation induced by substrate structure, J. Cryst. Growth 285 (2005) 400–407.
[7] B. Li, Y. Xie, M. Jing, G. Rong, Y. Tang, G. Zhang, In_2O_3 hollow microspheres:synthesis from designed $In(OH)_3$ precursors and applications in gas sensors and photocatalysis, Langmuir 22 (2006) 9380–9385.
[8] M. Kaur, N. Jain, K. Sharma, S. Bhattacharya, A.K. Mainak Roy, S.K. Tyagi, J.V. Gupta, M. Yakhmi, A.K. Roy, S.K. Tyagi, J.V. Gupta, Yakhmi, Room-temperature H_2S gas sensing at ppb level by single crystal In_2O_3 whiskers, Sens. Actuators B: Chem. 133 (2008) 456–461.
[9] Y. Chung, Y.S. Lee, D.D. Lee, Indium oxide thin film sensors for ozone monitoring produced by a sol–gel method, J. Mater. Sci. Lett. 22 (2003) 907–909.
[10] T. Yan, X. Wang, J. Long, P. Liu, X. Fu, G. Zhang, X. Fu, Urea-based hydrothermal growth, optical and photocatalytic properties of single-

crystalline $In(OH)_3$ nanocubes, J. Colloid Interf. Sci. 325 (2008) 425–431.
[11] Z.W. Pan, Z.R. Dai, Z.L. Wang, Nanobelts of semiconducting oxides, Science 291 (2001) 1947–1949.
[12] D. Calestani, M. Zha, A. Zappettini, L. Lazzarini, L. Zanotti, In-catalyzed growth of high-purity indium oxide nanowires, Chem. Phys. Lett. 445 (2007) 251–254.
[13] G. Cheng, E. Stern, S. Guthrie, M.A. Reed, R. Klie, Y. Hao, G. Meng, L. Zhang, Indium oxide nanostructures, Appl. Phys. A 85 (2006) 233–240.
[14] C.J. Chen, W.L. Xu, M.Y. Chern, Low-temperature epitaxial growth of vertical In_2O_3 nanowires on a-plane sapphire with hexagonal cross-section, Adv. Mater. 19 (2007) 3012–3015.
[15] G.Q. Ding, W.Z. Shen, M.J. Zheng, Z.B. Zhou, Indium oxide ''rods in dots'' nanostructures, Appl. Phys. Lett. 89 (2006) 063113.
[16] S.C. Chang, M.H. Huang, Formation of short In_2O_3 nanorod arrays within mesoporous silica, J. Phys. Chem. C 112 (2008) 2304–2307.
[17] Z.X. Cheng, X.B. Dong, Q.Y. Pan, J.C. Zhang, X.W. Dong, Preparation and characterization of In_2O_3 nanorods, Mater. Lett. 60 (2006) 3137–3140.
[18] K. Yura, K.C. Fredrikson, E. Matijevic, Preparation and properties of uniform colloidal indium compounds of different morphologies, Colloids Surf. 50 (1990) 281–293.
[19] C.H. Lee, M. Kim, T. Kim, A. Kim, J. Paek, J.W. Lee, S.Y. Choi, K. Kim, J.B. Park, K. Lee, Ambient pressure syntheses of size-controlled corundum-type In_2O_3 nanocubes, J. Am. Chem. Soc. 128 (2006) 9326–9327.
[20] S. Hamada, Y. Kudo, T. Kobayashi, Precipitation of uniform indium hydroxide particles from indium 2-aminobutyrato complex solutions, Colloids Surf. A 79 (1993) 227–232.
[21] A. Narayanaswamy, H. Xu, N. Pradhan, M. Kim, X. Peng, Formation of nearly monodisperse In_2O_3 nanodots and oriented-attached nanoflowers: hydrolysis and alcoholysis vs pyrolysis, J. Am. Chem. Soc. 128 (2006) 10310–10319.
[22] J. Du, M. Yang, S.N. Cha, D. Rhen, M. Kang, D.J. Kang, Indium hydroxide and indium oxide nanospheres, nanoflowers, microcubes, and nanorods: synthesis and optical properties, Cryst. Growth Des. 8 (2008) 2312–2317.
[23] R.B.H. Tahar, T. Ban, Y. Ohya, Y. Takahashi, Optical, structural, and electrical properties of indium oxide thin films prepared by the sol–gel method, J. Appl. Phys. 82 (1997) 865–870.
[24] Q. Tang, W. Zhou, W. Zhang, S. Ou, K. Jiang, W. Yu, Y.T. Qian, Size-controllable growth of single crystal $In(OH)_3$ and In_2O_3 nanocubes, Cryst. Growth Des. 5 (2005) 147–150.
[25] J. Yang, C. Lin, Z. Wang, J. Lin, $In(OH)_3$ and In_2O_3 nanorod bundles and spheres: microemulsion-mediated hydrothermal synthesis and luminescence properties, Inorg. Chem. 45 (2006) 8973–8979.
[26] H. Zhu, X. Wang, F. Yang, X. Yang, Template-free, surfactantless route to fabricate $In(OH)_3$ monocrystalline nanoarchitectures and their conversion to In_2O_3, Cryst. Growth Des. 8 (2008) 950–956.
[27] D. Yu, S.H. Yu, S. Zhang, J. Zuo, D.B. Wang, Y. Qian, Metastable hexagonal In_2O_3 nanofibers templated from InOOH nanofibers under ambient pressure, Adv. Funct. Mater. 13 (2003) 497–501.
[28] J. Huang, L. Gao, Anisotropic growth of $In(OH)_3$ nanocubes to nanorods and nanosheets via a solution-based seed method, Cryst. Growth Des 6 (2006) 1528–1532.
[29] Y. Zhang, J. Li, Q. Li, L. Zhu, X. Liu, X. Zhong, J. Meng, X. Cao, Preparation of In_2O_3 ceramic nanofibers by electrospinning and their optical properties, Scripta Mater. 56 (2007) 409–412.
[30] H. Jiang, K.S. Moon, Y. Sun, C.P. Wong, F. Hua, T. Pal, A. Pal, Tin/indium nanobundle formation from aggregation or growth of nanoparticles, J. Nanopart. Res. 10 (2008) 41–46.
[31] H. Zhang, X. Ren, Z. Cui, Shape-controlled synthesis of Cu_2O nanocrystals assisted by PVP and application as catalyst for synthesis of carbon nanofibers, J. Cryst. Growth 304 (2007) 206–210.
[32] D. Tao, W. Qian, Y. Huang, F. Wei, A novel low-temperature method to grow single-crystal ZnO nanorods, J. Cryst. Growth 271 (2004) 353–357.
[33] L. Guo, S. Yang, Synthesis and characterization of poly(vinylpyrrolidone)-modified zinc oxide nanoparticles, Chem. Mater. 12 (2000) 2268–2274.
[34] S. Giuffrida, L.L. Costanzo, G. Ventimiglia, C. Bongiorno, Photochemical synthesis of copper nanoparticles incorporated in poly(vinyl pyrrolidone), J. Nanopart. Res. 10 (2008) 1183–1192.
[35] S. Komarneni, D. Li, B. Newalkar, H. Katsuki, A.S. Bhalla, Microwave-polyol process for Pt and Ag nanoparticles, Langmuir 18 (2002) 5959–5962.
[36] S. Komarneni, H. Katsuki, D. Li, A.S. Bhalla, Microwave-polyol process for metal nanophases, J. Phys.-Condens. Matter 16 (2004) S1305–S1312.
[37] W.H. Ho, S.K. Yen, Preparation and characterization of indium oxide film by electrochemical deposition, Thin Solid Films 498 (2006) 80–84.